

ROA-BEV: 2D Region-Oriented Attention for BEV-based 3D Object Detection

Jiwei Chen¹, Yubao Sun², Laiyan Ding¹ and Rui Huang^{1*}

Abstract—Vision-based Bird’s-Eye-View (BEV) 3D object detection has recently become popular in autonomous driving. However, objects with a high similarity to the background from a camera perspective cannot be detected well by existing methods. In this paper, we propose a BEV-based 3D Object Detection Network with 2D Region-Oriented Attention (ROA-BEV), which enables the backbone to focus more on feature learning of the regions where objects exist. Moreover, our method further enhances the information feature learning ability of ROA through multi-scale structures. Each block of ROA utilizes a large kernel to ensure that the receptive field is large enough to catch information about large objects. Experiments on nuScenes show that ROA-BEV improves the performance based on BEVDepth. The source codes of this work will be available at <https://github.com/DFLYan/ROA-BEV>.

I. INTRODUCTION

The surround-view camera system is currently one of the most popular sensor systems in vision-based autonomous driving solutions. **Bird’s-Eye-View (BEV)** is a typically surround-view camera sensor system. This system generates a top-down view of the surrounding environment of the vehicle through the fusion of multiple cameras. Through the sensed images, autonomous vehicles can perform 3D object detection tasks to understand external scenes. It can detect the 3D attributes of objects, such as coordinates and size. A typical BEV-based 3D object detection model includes an image backbone, a **View Transformation Module (VTM)**, and a 3D object detection head. Specifically, the backbone contains a feature extraction module, such as ResNet [1], and a feature fusion module, such as **Feature Pyramid Networks (FPN)** [2]. The VTM is mainly used to project multi-view camera features onto the BEV plane.

However, extreme weather, varied illumination, or noise confuse objects and backgrounds, affecting the network’s perception capability. This phenomenon is particularly amplified in BEV representation, where features from all image regions are projected onto a single plane, causing severe information entanglement between foreground objects and complex backgrounds. Such spatial compression increases the difficulty of feature discrimination and leads to ambiguous positional priors for 3D detection. This motivates us to introduce 2D regions attention guidance to 1) enhance the backbone’s capability in distinguishing critical

objects through attention mechanisms, and 2) provide explicit structural priors from perspective-aware 2D regions results. Specifically, the per-view 2D regions establish reliable anchor points in image coordinates, which effectively constrain the search space for 3D detection and mitigate the learning ambiguity caused by BEV projection.

Therefore, in this work, we introduce a method called **2D Region-Oriented Attention for a BEV-based 3D Object Detection Network (ROA-BEV)**, intended to enable the image feature extractor of the network to focus more on learning where objects exist, thereby reducing interference from other background information. In order to generate more accurate regions, we directly use multi-scale features from the feature extractor and fuse the generated results. Meanwhile, each scale of network uses large kernel convolution to capture information. The convolutional kernel of the large receptive field better balances the learning background and foreground, as well as the contextual relationships between objects in the foreground. In summary, the major contributions of this paper are:

- We propose ROA-BEV to enable the network to focus on extracting features of regions where objects exist and separate them from background, and it is applicable to the previous BEV methods.
- We propose ROA to generate regions of objects in camera views, which fuses multi-scale features from the image backbone. Large kernel is used on every scale to catch more information, especially on large objects.
- Our method is validated to be effective in experiments based on BEVDepth [3] on the nuScenes val set.

II. RELATED WORK

A. Vision-based 3D Object Detection

The key challenge of vision-based 3D object detection is the inherent ambiguity in estimating depth from images. Despite this, significant progress has been made through various approaches. One prominent direction involves predicting 3D bounding boxes from 2D image features. Early works, such as CenterNet [4], demonstrates that 2D detectors can be adapted for 3D detection with minimal modifications. FCOS3D [5] converts 3D targets to the image domain for predicting both 2D and 3D attributes. DD3D [6] further emphasizes the benefit of depth pretraining. Another active research line focuses on projecting 2D image features into 3D space. LSS pioneers the view transform method, predicting depth distributions and projecting features onto BEV. BEVDet [7] utilizes the BEV feature space for 3D detection. BEVDet4D [8] combines multiple frames of temporal

*Corresponding author

¹Jiwei Chen, Laiyan Ding and Rui Huang are with School of Science and Engineering, The Chinese University of Hong Kong, Shenzhen 518172, China (e-mail: {jiweichen2, laiyanding, ruihuang}@link.cuhk.edu.cn).

²Yubao Sun is with the Engineering Research Center of Digital Forensics, Ministry of Education, Nanjing University of Information Science and Technology, Nanjing 210044, China (e-mail: sunyb@nuist.edu.cn)

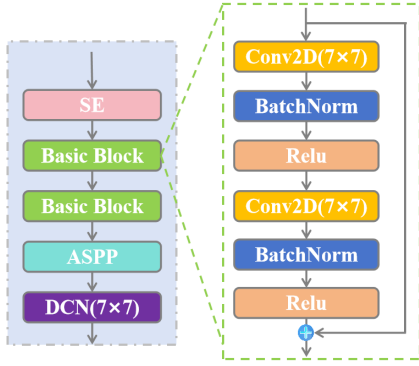


Fig. 2: Details of the Large Kernel Basic (LKB) module in the ROA.

features from the FPN network, to produce features more focused on potential object areas. Subsequently, similar to BEVDepth, these image features are utilized for viewpoint transformation and subsequent detection head.

B. Multi-scale 2D Region Oriented Attention

In the forward feature extraction process, objects of different scales have different expressions in different layers, accompanied by information loss. We utilize features from four scales within the backbone, inputting each into the **Large Kernel Basic(LKB)** module. The detail of ROA is illustrated in the red dashed box of Fig. 1. Subsequently, four scaled features are either upsampled or downsampled to match the FPN network before being summed. The details of processing multi-scale 2D ROA can be formulated as:

$$\begin{aligned} \mathcal{O}_{ROA} = & DS(\mathcal{F}_{LKB}^{\xi_1}(\mathcal{O}_{backbone}^1), 4) \\ & + DS(\mathcal{F}_{LKB}^{\xi_2}(\mathcal{O}_{backbone}^2), 2) \\ & + \mathcal{F}_{LKB}^{\xi_3}(\mathcal{O}_{backbone}^3) \\ & + U(\mathcal{F}_{LKB}^{\xi_4}(\mathcal{O}_{backbone}^4), 2) \end{aligned} \quad (1)$$

where $DS(input, s)$ denotes downsampling the features by s times and $U(input, s)$ denotes upsampling the features by s times. \mathcal{F}_{LKB}^{ξ} represents the LKB module. $\mathcal{O}_{backbone}^i$ denotes the output of i -th scale in the backbone.

Finally, the generated 2D ROA will be element-wise multiplied by the output of FPN. The attention mechanism can be formulated as:

$$\mathcal{O}_{feature} = \mathcal{O}_{FPN} \times \mathcal{O}_{ROA} \quad (2)$$

C. Large Kernel Basic Module

As shown in Fig. 2, the Large Kernel Basic (LKB) module is modified on DepthNet in BEVDepth, which contains Squeeze-and-Excitation (SE) [18], Basic block, Atrous Spatial Pyramid Pooling (ASPP) [19], and Deformable Convolution Network (DCN) [20]. However, different from the DepthNet, the kernel size of every basic block and DCN is 7×7 . These large kernel convolutions, characterized by their extended receptive fields, enable the model to capture a broader context and spatial relationships within the input data, enhancing feature extraction capabilities.

Although DCN introduces deformability to adapt to input shape changes, the benefits of the large kernel convolutions used earlier in the model are still evident, as they contribute to the overall robustness and feature discriminability.

D. 2D ROA Label Generation

Algorithm 1 Ground Truth Generation of ROA

Require: 3D labels of objects in one frame $List\{B_{3D}\}$, extrinsic $\{\mathcal{R}, \mathcal{T}\}$ and intrinsic $\{\mathcal{K}\}$ of cameras

- 1: Initialize $GT_{ROA} = 0.1 \times \mathbf{1}_{Cameras \times H \times W}$
- 2: **for** each 3D bounding box B_{3D} in $List\{B_{3D}\}$ **do**
- 3: **for** each camera index i **do**
- 4: Coordinate system transformation:
- 5: $B' \leftarrow [\mathcal{R}_i \ \mathcal{T}_i] B_{3D}$
- 6: $B_{2D} \leftarrow \mathcal{K}_i B'$
- 7: **if** B_{2D} is within the i -th camera FOV **then**
- 8: Calculate the corners of 2D bounding box in the camera i :
- 9: $x_{min}, y_{min}, x_{max}, y_{max} \leftarrow B_{2D}$
- 10: Update GT of ROA:
- 11: $GT_{ROA}[i][y_{min} : y_{max}, x_{min} : x_{max}] += 1.0$
- 12: **end if**
- 13: **end for**
- 14: **end for**
- 15: **return** The ground Truth of ROA GT_{ROA}

As illustrated in the bottom blue box of Fig. 1, we transform the 3D coordinates of the target within the ego coordinate system into 2D coordinates in the camera coordinate system using the camera's extrinsic and intrinsic parameters. Subsequently, we initialize six matrices to all zeros, one for each camera, and draw frames in these matrices based on the 2D labels. It should be noted that in order to prevent the impact of all zero matrices on network convergence, we add 0.1 to the initialized matrix. The area within the frame is assigned the value of 1. If the same pixel is enclosed by different boxes multiple times, the values at that pixel are cumulatively added. The complete process is summarized in Algorithm 1.

E. Training Loss

This section introduces the loss function. As shown in Fig. 1, our method has three major branches to be supervised: Detection Head, DepthNet and ROA. Therefore, we define three functions to minimize: \mathcal{L}_{Det} , \mathcal{L}_{Depth} and \mathcal{L}_{ROA} . The total loss can be formulated as:

$$\mathcal{L} = \mathcal{L}_{Det} + \lambda_1 \mathcal{L}_{Depth} + \lambda_2 \mathcal{L}_{ROA} \quad (3)$$

where λ_1 denotes the weight of depth loss, λ_2 denotes the weight of ROA loss. \mathcal{L}_{Det} and \mathcal{L}_{Depth} follow BEVDepth. \mathcal{L}_{ROA} is the ROA loss function for the supervision of the proposed ROA branch. We use \mathcal{L}_1 loss to minimize the \mathcal{L}_{roa} :

$$\mathcal{L}_{ROA} = \mathcal{L}_1\{\mathcal{O}_{ROA}, GT_{ROA}\} \quad (4)$$

where GT_{ROA} denotes the ground truth of 2D Region Attention in the Fig. 1.

TABLE I: Comparison on the nuScenes val set. All results are trained with CBGS [21]

Method	Backbone	Resolution	mAP \uparrow	NDS \uparrow	mATE \downarrow	mASE \downarrow	mAOE \downarrow	mAVE \downarrow	mAAE \downarrow
PETR [11]	R50	384 \times 1056	0.313	0.381	0.768	0.278	0.564	0.923	0.225
BEVDet [7]	R50	256 \times 704	0.298	0.379	0.725	0.279	0.589	0.860	0.245
BEVDet4D [8]	R50	256 \times 704	0.322	0.457	0.703	0.278	0.495	0.354	0.206
BEVDepth [3]	R50	256 \times 704	0.351	0.475	0.639	0.267	0.479	0.428	0.198
ROA-BEV	R50	256 \times 704	0.361	0.485	0.640	0.269	0.459	0.374	0.212

F. Dataset and Metrics

IV. EXPERIMENTS

The nuScenes dataset¹ [22] stands as a significant benchmark for autonomous driving research. This dataset encompasses 750 scenarios for training, 150 for validation, and another 150 for testing. The data encompasses inputs from six cameras, one LiDAR, and five radars, capturing the multimodal nature of the driving environment. For 3D object detection task, the nuScenes Detection Score (NDS) is a crucial metric, integrating various performance aspects beyond the traditional mean Average Precision (mAP). The NDS considers additional true positive metrics, including mean Average Translation Error (mATE), mean Average Scale Error (mASE), mean Average Orientation Error (mAOE), mean Average Velocity Error (mAVE), and mean Average Attribute Error (mAAE).

A. Implementation Details

We utilize BEVDepth [3] as our baseline. All experiments are trained and tested with 8 NVIDIA GeForce RTX 2080ti GPUs. Batch size is set to 2 in each GPU. We employ ResNet-50 [1] as the image backbone and the image resolution is 704*256. Our models are trained using the AdamW [23] optimizer, and gradient clipping is applied. When compared to other methods in the Table I, all results are obtained with CBGS [21]. The epoch of the training stage is 20. The initial learning rate is 2e-4. Learning rate decays occur at epochs 10, 14, and 18. Each update reduces the learning rate to 0.6 times the previous rate. For the ablation study, all models are trained 40 epochs without CBGS, and the learning rate is 1.5e-4. Other settings are the same. λ_1 and λ_2 are set to 3 and 1 separately. All experiments are implemented based on MMDetection3D [24].

B. Main Results

1) *Comparison with State-of-the-Arts*: In our experiments, we apply CBGS [21] to various 3D object detection methods and evaluate their performance on a standard benchmark, which is presented in the Table I. Our method achieves the highest mAP and NDS scores among all the compared methods, indicating its effectiveness in improving the overall detection performance.

2) *Visualization*: This section will show the visualization of detection results. The results are shown in the Fig. 3. We provide two examples to demonstrate the effectiveness of our method. In each example, the advantages of our method are marked with red circles. In the first example,

the truck in the distance merges with the white clouds in the sky and the black ground. Our method successfully detects the truck. Similarly, our method successfully detects objects under backlighting in the second example. Moreover, the category is correct for cars, while BEVDepth’s prediction results miss the car and identify another car as a truck. To verify the effectiveness of ROA, we visualize the ROA results generated by the network. As shown in the Fig. 4, the distant truck region can be generated. The distant truck blends well with the background, resulting in poor feature extraction from the backbone. Therefore, the output of ROA increases the weight of the corresponding position accordingly. On the contrary, the backbone can be extracted better for the car on the right, and the ROA results give smaller weights to compensate for the features.

C. Ablation Study

TABLE II: Ablation study of using ROA and type of region on nuScenes val.

	ROA	Type of Region	mAP \uparrow	NDS \uparrow
Baseline	×	×	0.329	0.443
Ours	✓	×	0.335	0.450
	✓	Binary-Pre	0.338	0.454
	✓	Overlap-Pre	0.349	0.461
	×	Binary-GT	0.374	0.471
	×	Overlap-GT	0.411	0.490

1) *Component Analysis*: We evaluate the performance of our proposed method against the baseline BEVDepth model on various metrics. The results in the Table II demonstrate that incorporating attention supervision significantly enhances the model’s performance. Specifically, using the proposed ROA module but without additional ground truth (GT) supervision achieves an improvement in mAP (from 0.329 to 0.335) and NDS (from 0.443 to 0.450) compared to the baseline, BEVDepth, indicating better overall detection accuracy. Furthermore, when using the binary ROA label to supervise the ROA, mAP increases to 0.338 and NDS to 0.454. Detailly, the binary label means changing the value of the overlap label to binarization. The above results show that using attention supervision can improve the detection results of the network. Specifically, if multiple objects overlap, using overlap instead of binary GT supervision can avoid the network mistaking multiple objects for one and improve network performance.

Furthermore, we experiment with the upper limit of network performance using ROA, which is the GT directly inputted into ROA. The trend of results is the same: with the use of overlap, it can achieve optimal network performance.

¹<https://www.nuscenes.org>

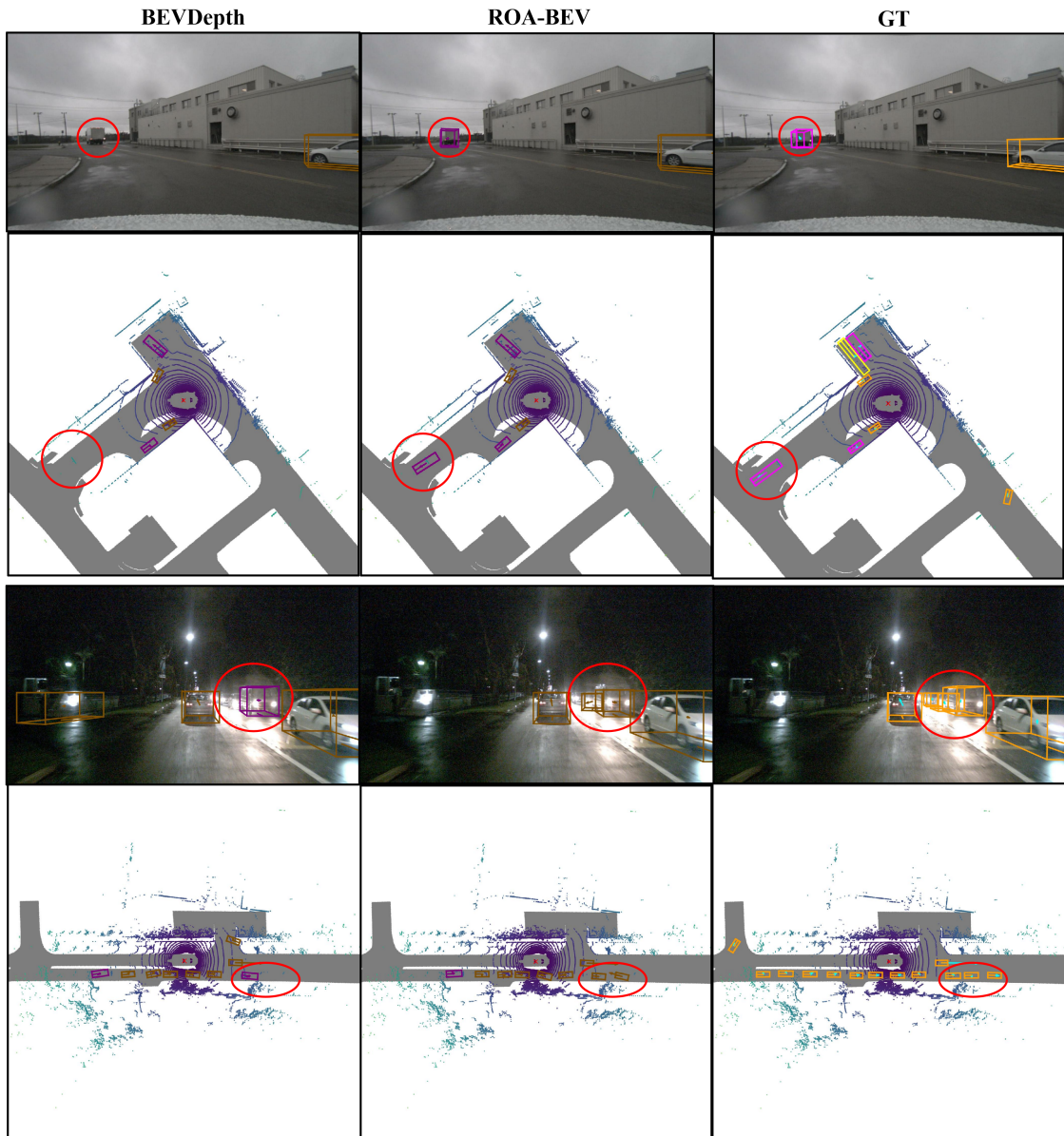


Fig. 3: Visualization of detection results on images and BEV view.

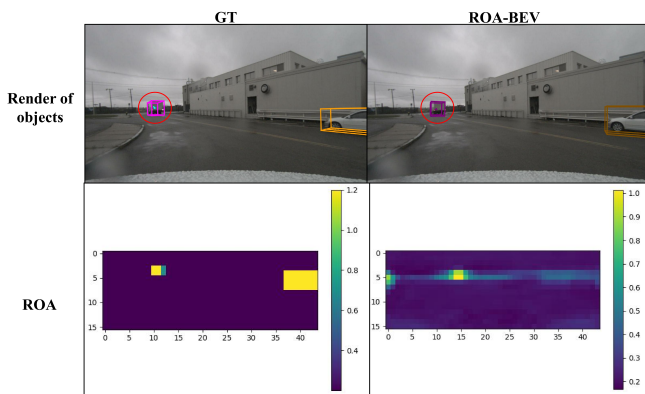


Fig. 4: Visualization of ROA.

In addition, by comparing the results predicted using GT and network, it can be seen that there is still a gap of 0.062 and 0.029 in mAP and NDS. This indicates that the method has the potential for further research and development.

2) *Specific Classes Analysis:* In our experiments, we evaluate the performance of our proposed method by integrating it with two 3D object detection frameworks: BEVDet [7] and BEVDepth [3]. The results, presented in the TABLE III, demonstrate the effectiveness of our approach in enhancing detection accuracy across various categories of objects. For BEVDet, our method consistently improves the detection accuracy for most object categories, with notable percentage increases in categories such as 'construction_vehicle' (+12.82%) and 'motorcycle' (+11.57%). Similarly, when integrated with BEVDepth, our approach

TABLE III: Ablation study of using ROA on different methods. "construc." denotes the category of construction vehicle.

		BEVDet [7]	BEVDet [7] +ROA	Difference	Percentage	BEVDepth [3]	BEVDepth [3] +ROA	Difference	Percentage
mAP	car	0.517	0.528	0.011	2.13%	0.493	0.511	0.018	3.74%
	truck	0.226	0.243	0.017	7.52%	0.258	0.280	0.0221	8.57%
	bus	0.305	0.328	0.023	7.54%	0.362	0.399	0.037	10.28%
	trailer	0.101	0.105	0.004	3.96%	0.153	0.18	0.027	17.57%
	construc.	0.039	0.044	0.005	12.82%	0.056	0.068	0.012	21.86%
	pedestrian	0.318	0.340	0.022	6.92%	0.357	0.375	0.018	4.92%
	motorcycle	0.216	0.241	0.025	11.57%	0.308	0.316	0.008	2.46%
	bicycle	0.203	0.199	-0.004	-1.97%	0.308	0.311	0.003	1.04%
	traffic cone	0.499	0.511	0.012	2.40%	0.492	0.524	0.032	6.57%
	barrier	0.404	0.436	0.0320	7.92%	0.505	0.523	0.019	3.67%
Average	0.283	0.298	0.015	5.20%	0.329	0.349	0.020	5.92%	
NDS	Average	0.350	0.368	0.018	5.11%	0.443	0.461	0.018	3.95%

leads to substantial improvements, particularly in categories like 'construction_vehicle' (+21.86%), 'trailer' (+17.57%) and 'bus' (+10.28%). It is worth noting that while there is a minor decrease in performance for one category, 'bicycle' with BEVDet. We consider that the possible reason is that their thin, narrow shape gets more easily distorted when converting to the BEV, combined with fewer bicycle examples in our training data. However, the overall trend of the mAP and NDS scores indicates a positive impact on detection accuracy, with improvements of 5.20% and 5.11% respectively for BEVDet, and 5.92% and 3.95% for BEVDepth. These results underscore the efficacy of our method in enhancing the performance of existing 3D object detection models, particularly in challenging scenarios involving small or partially occluded objects.

3) *Multi-scale Analysis*: We analyze the impact of different feature extraction methods. The results in the Table IV indicate that incorporating multi-scale features yields the best performance. These findings underscore the importance of utilizing multi-scale features directly from the backbone, as this structure can reduce the loss of information transmission after FPN.

TABLE IV: Ablation study of using multi-scale features.

Input of the ROA feature	mAP↑	NDS↑
Same scale from backbone	0.332	0.451
FPN backbone	0.345	0.453
Multi-scale from backbone	0.349	0.461

TABLE V: Ablation study of using different size of kernel.

Kernel size of basic block	mAP↑	NDS↑
3*3	0.342	0.457
5*5	0.339	0.450
7*7	0.349	0.461
9*9	0.335	0.450
11*11	0.334	0.449

4) *Kernel Size Analysis*: We investigate the impact of varying kernel sizes in the basic block. The results, presented in the Table V, a kernel size of 7 achieves the highest mAP and NDS with a value of 0.349 and 0.461 separately. This suggests that the 7×7 kernel size aids in capturing more contextual information, simultaneously balancing parameter quantity and accuracy

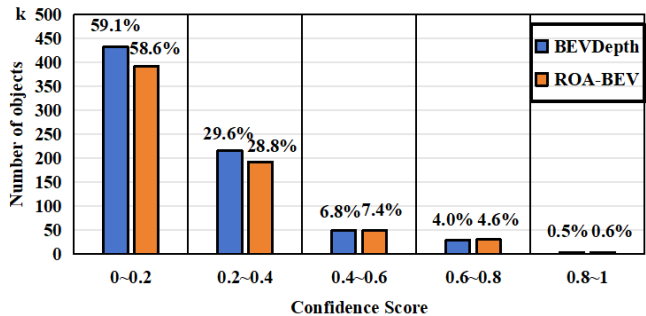


Fig. 5: Comparison of the distribution of results. The total results predicted by BEVDepth [3] and ROA-BEV are 731992 and 667578, respectively.

5) *Results Distribution Analysis*: As shown in the Fig. 5, the number of predicted results has significantly decreased. Meanwhile, the proportion of high confidence prediction results has also increased.

D. Conclusion

In this paper, we propose ROA-BEV to orient feature extraction to focus on object regions in camera views. ROA fusions multi-scale features of images to generate attention regions. LKB in ROA increases the receptive field to enhance the network's performance between the background and objects, as well as the relationships between different objects. The ROA supervisor does not need additional data because the ROA label is projected from a 3D label. ROA-BEV can be embedded into most BEV-based 3D object detection methods.

However, some limitations also exist in our method. The performance of ROA has a significant impact on the final 3D object detection results. Errors and omissions in the region can reinforce unfavorable information and mislead the network. Given that there is still a significant gap between the existing results and the use of GT, improving network efficiency is an area that can be studied in the future.

REFERENCES

- [1] K. He, X. Zhang, S. Ren, and J. Sun, "Deep residual learning for image recognition," in *Proceedings of the IEEE conference on computer vision and pattern recognition*, 2016, pp. 770–778.
- [2] T.-Y. Lin, P. Dollár, R. Girshick, K. He, B. Hariharan, and S. Belongie, "Feature pyramid networks for object detection," in *Proceedings of the IEEE conference on computer vision and pattern recognition*, 2017, pp. 2117–2125.
- [3] Y. Li, Z. Ge, G. Yu, J. Yang, Z. Wang, Y. Shi, J. Sun, and Z. Li, "Bevdepth: Acquisition of reliable depth for multi-view 3d object detection," in *Proceedings of the AAAI Conference on Artificial Intelligence*, vol. 37, no. 2, 2023, pp. 1477–1485.
- [4] K. Duan, S. Bai, L. Xie, H. Qi, Q. Huang, and Q. Tian, "Centernet: Keypoint triplets for object detection," in *Proceedings of the IEEE/CVF international conference on computer vision*, 2019, pp. 6569–6578.
- [5] T. Wang, X. Zhu, J. Pang, and D. Lin, "Fcos3d: Fully convolutional one-stage monocular 3d object detection," in *Proceedings of the IEEE/CVF International Conference on Computer Vision*, 2021, pp. 913–922.
- [6] D. Park, R. Ambrus, V. Guizilini, J. Li, and A. Gaidon, "Is pseudolidar needed for monocular 3d object detection?" in *Proceedings of the IEEE/CVF International Conference on Computer Vision*, 2021, pp. 3142–3152.
- [7] J. Huang, G. Huang, Z. Zhu, Y. Ye, and D. Du, "Bevdet: High-performance multi-camera 3d object detection in bird-eye-view," *arXiv preprint arXiv:2112.11790*, 2021.
- [8] J. Huang and G. Huang, "Bevdet4d: Exploit temporal cues in multi-camera 3d object detection," *arXiv preprint arXiv:2203.17054*, 2022.
- [9] Y. Wang, V. C. Guizilini, T. Zhang, Y. Wang, H. Zhao, and J. Solomon, "Detr3d: 3d object detection from multi-view images via 3d-to-2d queries," in *Conference on Robot Learning*. PMLR, 2022, pp. 180–191.
- [10] Z. Li, W. Wang, H. Li, E. Xie, C. Sima, T. Lu, Y. Qiao, and J. Dai, "Bevformer: Learning bird's-eye-view representation from multi-camera images via spatiotemporal transformers," in *European conference on computer vision*. Springer, 2022, pp. 1–18.
- [11] Y. Liu, T. Wang, X. Zhang, and J. Sun, "Petr: Position embedding transformation for multi-view 3d object detection," in *European Conference on Computer Vision*. Springer, 2022, pp. 531–548.
- [12] Z. Liu, Y. Lin, Y. Cao, H. Hu, Y. Wei, Z. Zhang, S. Lin, and B. Guo, "Swin transformer: Hierarchical vision transformer using shifted windows," in *Proceedings of the IEEE/CVF international conference on computer vision*, 2021, pp. 10 012–10 022.
- [13] Z. Liu, H. Mao, C.-Y. Wu, C. Feichtenhofer, T. Darrell, and S. Xie, "A convnet for the 2020s," in *Proceedings of the IEEE/CVF conference on computer vision and pattern recognition*, 2022, pp. 11 976–11 986.
- [14] F. Chabot, M. Chaouch, J. Rabarisoa, C. Teuliere, and T. Chateau, "Deep manta: A coarse-to-fine many-task network for joint 2d and 3d vehicle analysis from monocular image," in *Proceedings of the IEEE conference on computer vision and pattern recognition*, 2017, pp. 2040–2049.
- [15] J. Ku, A. D. Pon, and S. L. Waslander, "Monocular 3d object detection leveraging accurate proposals and shape reconstruction," in *Proceedings of the IEEE/CVF conference on computer vision and pattern recognition*, 2019, pp. 11 867–11 876.
- [16] Y. Lu, X. Ma, L. Yang, T. Zhang, Y. Liu, Q. Chu, J. Yan, and W. Ouyang, "Geometry uncertainty projection network for monocular 3d object detection," in *Proceedings of the IEEE/CVF International Conference on Computer Vision*, 2021, pp. 3111–3121.
- [17] X. Jiang, S. Li, Y. Liu, S. Wang, F. Jia, T. Wang, L. Han, and X. Zhang, "Far3d: Expanding the horizon for surround-view 3d object detection," in *Proceedings of the AAAI Conference on Artificial Intelligence*, vol. 38, no. 3, 2024, pp. 2561–2569.
- [18] J. Hu, L. Shen, and G. Sun, "Squeeze-and-excitation networks," in *Proceedings of the IEEE conference on computer vision and pattern recognition*, 2018, pp. 7132–7141.
- [19] L.-C. Chen, G. Papandreou, I. Kokkinos, K. Murphy, and A. L. Yuille, "Deeplab: Semantic image segmentation with deep convolutional nets, atrous convolution, and fully connected crfs," *IEEE transactions on pattern analysis and machine intelligence*, vol. 40, no. 4, pp. 834–848, 2017.
- [20] J. Dai, H. Qi, Y. Xiong, Y. Li, G. Zhang, H. Hu, and Y. Wei, "Deformable convolutional networks," in *Proceedings of the IEEE international conference on computer vision*, 2017, pp. 764–773.
- [21] B. Zhu, Z. Jiang, X. Zhou, Z. Li, and G. Yu, "Class-balanced grouping and sampling for point cloud 3d object detection," *arXiv preprint arXiv:1908.09492*, 2019.
- [22] H. Caesar, V. Bankiti, A. H. Lang, S. Vora, V. E. Liong, Q. Xu, A. Krishnan, Y. Pan, G. Baldan, and O. Beijbom, "nusenes: A multimodal dataset for autonomous driving," in *Proceedings of the IEEE/CVF conference on computer vision and pattern recognition*, 2020, pp. 11 621–11 631.
- [23] I. Loshchilov, "Decoupled weight decay regularization," *arXiv preprint arXiv:1711.05101*, 2017.
- [24] M. Contributors, "MMDetection3D: OpenMMLab next-generation platform for general 3D object detection," <https://github.com/open-mmlab/mmdetection3d>, 2020.